Self-assembling network and bundle structures in systems of rods and crosslinkers – A Monte Carlo study

Raghunath Chelakkot,[ab] Reinhard Lipowsky[a] and Thomas Gruhn*[ac]

Received 21st May 2008, Accepted 2nd December 2008
First published as an Advance Article on the web 23rd January 2009
DOI: 10.1039/b808580c

Self-assembling structures are studied in a binary system of long and short spherocylinders. The short spherocylinders have an adhesive site on both ends with which they can bind to the long spherocylinders. In this way, they act as crosslinkers that may interconnect a pair of long rods. With the help of Monte Carlo simulations, the structure of crosslinker-mediated rod assemblies is studied as a function of rod and crosslinker concentrations, and of the adhesive strength between the two. Though the system is rather simple compared to networks of crosslinked filaments in the cytoskeleton, it shows a complex phase behaviour, including the formation of bundles of parallel rods and a transition to a three-dimensional, low-density network. These bundles occur both in percolated and non-percolated systems. In a certain range of rod and crosslinker concentrations, the amount of bundling rods is a non-monotonic function of the adhesive strength. The percolation boundary has been determined and the dependence of bundle formation on the system parameters has been studied systematically.

1. Introduction

Systems of rigid rods show a large variety of self-organized structures. Most analytical and numerical studies of rigid rod systems are based on hard spherocylinders. For monodisperse systems of hard spherocylinders the full phase diagram is known and includes an isotropic (I), a nematic (N), and a smectic A (SmA) phase.[1] More complex structures are formed in binary systems of hard spherocylinders. The phase diagrams of binary rod systems exhibit additional phase coexistence regions, which involve a partial demixing of the rods. Systems of spherocylinders with the same length but different diameters have been studied extensively by analytical methods and simulations.[2–6] In these studies, I–I, I–N, and N–N phase coexistence regions were observed. As shown with extended Onsager theory, I–I coexistence is excluded for binary systems of hard spherocylinders with the same diameters but different lengths.[7] Cinacchi *et al.* have used density functional theory to calculate a detailed phase diagram for systems of hard spherocylinders with different lengths.[8] It comprises various smectic A_2 phases, in which the two rod components form subpatterns in the smectic layers. An overview over the phase behavior of binary hard rod systems is given in ref. 9.

More complex structures occur in systems of hard rods with attractive interactions. These latter systems have hardly been investigated so far. Thermodynamic properties of systems of short hard spherocylinders with dipoles or quadrupoles have been studied in Monte Carlo simulations by Janeček and Boublík.[10] McGrother and coworkers have investigated the phase behavior of hard spherocylinders with an attractive potential at one end that leads to the formation of dimers.[11]

Recently, we have presented simulation results for a system of hard spherocylinders with adhesive ends.[12] The system shows spontaneous formation of a scaffold-like network, in which, locally, the rods form tetragonal structures. Self-assembling networks of rods are of great relevance for various nano-technological applications for which self-organized colloidal rods can be used to build nano-circuits, transistors or biosensors.[13–15]

In this article, we investigate a binary system that consists of long and short spherocylinders. The short spherocylinders have an adhesion site at each end, with which they can bind to the long spherocylinders. In the following, the short spherocylinders are denoted as 'crosslinkers' while the long ones are named 'rods'. Since a crosslinker can bind to two rods, a network of interconnected rods can form.

Our model system is inspired by the cytoskeleton of living cells, where long actin filaments (F-actin) and microtubule (MT) filaments are interconnected by various types of binding proteins.[16] Crosslinking proteins such as α-actinin and myosin-II adhere to F-actin and MTs and assemble them into various intracellular structures. Mechanical properties, such as elastic shear moduli, vary strongly with the concentration of actin and crosslinking proteins.[17–22] The structure of filament assembly ranges from dilute networks of isotropically oriented filaments to dense bundles, in which filaments are closely packed and nearly parallel to each other.[16,23] It has been shown that proteins in the spectrin superfamily, such as α-actinin, assemble the F-actin filaments into both bundles and networks, depending on their concentration and their affinity towards F-actin.[21,24] With a dilute concentration of crosslinkers, the filaments are assembled into a dilute isotropic network. When the α-actinin concentration is increased, the filaments form bundles.[21,22,24]

[a]*Max Planck Institute for Colloids and Interfaces, Science Park Golm, D-14424 Potsdam, Germany. E-mail: gruhn@uni-mainz.de*
[b]*Institut für Festkörperforschung, Forschungszentrum Jülich, Jülich, Germany*
[c]*Johannes Gutenberg University, Staudinger Weg 9, D-55128 Mainz, Germany*

Several previous investigations have addressed model systems that mimic certain aspects of cytoskeletal networks. The interactions mediated between the crosslinkers lead to effective filament–filament interactions that depend, in general, both on the filament separation and on their orientation.[25] Using such effective interactions together with modified Onsager theory, Borukhov *et al.* have studied an equilibrium model system of F-actin and crosslinking proteins.[26] Zilman and Safran[27] have analyzed the influence of branching and capping proteins on the assembling of actin monomers. Other theoretical studies are dedicated to dynamic aspects, like non-equilibrium pattern formation in a system of MTs and molecular motors,[28–32] or the growth kinetics of actin filaments.[33,34]

In this article, we investigate a binary system of crosslinkers and rods and study how the assembly of bundles and network-like structures depends on the rod volume fraction, the crosslinker–rod ratio, and the adhesion strength of the crosslinker–rod interaction. The comparatively simple model system is inspired by crosslinked actin filaments but differs in many respects from the complex properties of actin networks: The long rods in our system are rigid and have a constant, unique length that is 15 times the rod diameter. Actin filaments are semi-flexible[35] and have a broad length distribution which is typically exponential but is qualitatively different for filaments in crosslinked bundles.[36,37] Many properties, like the percolation threshold, depend on the length distribution,[38,39] while other aspects such as the critical behavior at the percolation point should be widely independent of the rod lengths, or may change only quantitatively. Our model system is restricted to hard repulsions and short-range attractive potentials, while counterion-induced long-range interactions are neglected.[40,41] The crosslinkers are rigid rods rather than flexible proteins, no directed walks of active motors are considered, and the rods have no polarity. In this paper we show which system properties can be found in a simple system of long rods and crosslinkers. The system shows a comparably rich phase diagram of low-density three-dimensional structures that include a percolation transition towards a spanning network and the formation of bundles. The observed structures can uniquely be ascribed to steric interactions and the crosslinking mechanism.

The obtained phase diagrams reveal the dependence of network and bundle structures on the rod and crosslinker concentration and the adhesive strength. To the best of our knowledge, these are the first computer simulations of a rod network model in which crosslinkers are explicitly included.

The article is organized as follows: In Section 2, the model system is introduced. The percolation transition of the rod networks is investigated in Section 3. The formation of bundles is analyzed in Section 4. Simulation results are collected in the phase diagrams, presented in Section 5. A summary is given in Section 6.

2. Model and simulation methods

The model system consists of two types of spherocylinders, which represent the rods (r) and the crosslinking proteins (l) see, Fig. 1(a). The spherocylinders consist of a cylinder of diameter D capped at both ends by a hemisphere of the same diameter. The configuration of a spherocylinder j is determined by its position of the center of mass $\mathbf{r}_j$ and the unit vector $\mathbf{u}_j$ parallel to the cylinder axis. The cylinder axis, which points from $\mathbf{r}_j - \frac{L(j)}{2}\mathbf{u}_j$ to $\mathbf{r}_j + \frac{L(j)}{2}\mathbf{u}_j$ has a length $L(j) = L_r$, if j represents a rod, and $L(j) = L_l$, if it represents a crosslinker. Each pair of spherocylinders interact *via* a repulsive hard-core potential

$$U_{hc}(\lambda_{ij}) \equiv \begin{cases} 0 & \text{if } \lambda_{ij} \geq d \\ \infty & \text{if } \lambda_{ij} < d \end{cases} \tag{1}$$

where λ_{ij} is the shortest distance between the spherocylinder axes, which is

$$\lambda_{ij} \equiv \min_{\substack{-1\leq s_i\leq 1 \\ -1\leq s_j\leq 1}} \left\| \left(\mathbf{r}_j + \frac{s_j L(j)}{2}\mathbf{u}_j\right) - \left(\mathbf{r}_i + \frac{s_i L(i)}{2}\mathbf{u}_i\right) \right\| \tag{2}$$

In addition, a rod i and the rod-adhering sites of a crosslinker j interact through an attractive site–site potential. The attractive interaction is realized by a square-well potential, which is defined as a function of the shortest distance σ_{ij}, between the adhesive sites and the rod axis

$$U_{sw}(\sigma_{ij}) \equiv \begin{cases} -\varepsilon & \text{if } \sigma_{ij} < a \\ 0 & \text{if } \sigma_{ij} \geq a \end{cases} \tag{3}$$

The two ends of the crosslinkers are distinguished by the two labels + and −. The shortest distances σ_{ij}^{+} and σ_{ij}^{-} between the adhering sites of the crosslinker and the axis of the rod are given by

$$\sigma_{ij}^{\pm} \equiv \min_{-1\leq s_i\leq 1} \left\| \mathbf{q}_j^{\pm} - \left(\mathbf{r}_i + \frac{s_i L_r}{2}\mathbf{u}_i\right) \right\| \tag{4}$$

with the adhering sites located at $\mathbf{q}_j^{\pm} \equiv \mathbf{r}_j \pm d\mathbf{u}_j$, see Fig. 1(b). Here, d is the distance between the center of the crosslinker and the rod adhering sites, which are located symmetrically on both ends of the spherocylinder axis of the crosslinker.

The total interaction potential between a rod and a crosslinker is given by

$$U_{ij}^{rl} = U_{hc}(\lambda_{ij}) + U_{sw}(\sigma_{ij}^{+}) + U_{sw}(\sigma_{ij}^{-}) \tag{5}$$

In our simulations, the rods have length $L_r = 15D$ while the crosslinker length is $L_l = 2D$. The square-well diameter a, which defines the range of the rod-adhering potential of the crosslinker, is set to $a = 0.7D$. The square-well potentials were placed symmetrically along the cylindrical axes, at a distance $d = 1.35D$ from the center of mass of the crosslinker. Since the range a of the attractive sites is smaller than the diameter D of the spherocylinders, one rod cannot adhere to both attractive sites of a crosslinker. Furthermore, due to the location and the range of the attractive sites, the angle θ_{lr} between a rod and an adhering crosslinker is typically close to $\pi/2$. In general, attractive interaction between a rod and a crosslinker requires $\theta_{lr} \gtrsim \pi/3$.

Simulations are performed for systems of N_r rods and N_l crosslinkers. The systems can be characterized by the following three parameters,

(i) the adhesive strength ε,

(ii) the number n_{lr} of crosslinkers per rod, with $n_{lr} \equiv N_l / N_r$, and

(iii) the volume fraction ϕ of the rods, with $\phi \equiv N_f v_r / V$. Here, v_r is the volume of the spherocylindrical rod, which is equal to $v_r \equiv \frac{1}{6}\pi D^3 + \pi D^2 L_r$, and V is the total volume of the system.

The values of ϕ and n_{lr} were determined by choosing suitable values of N_r, N_l and V which were kept fixed during the simulation run. Simulations were performed for values of ϕ between 0.003 and 0.05 and of n_{lr} between 0.5 and 6. The length of the rods sets a lower limit to the simulation box size, and the side length $V^{1/3}$ is always set to be greater than $2L_r$. In the Monte Carlo simulations, new configurations are generated by translational and rotational moves of the rods and crosslinkers. For a system of N_r rods and N_l crosslinkers, $2(N_r + N_l)$ attempts of an orientational or translational move are made every sweep.

Starting from a lattice configuration, an isotropic state is achieved by equilibrating the system in the absence of attractive interactions, *i.e.* for $\varepsilon = 0$, using a constant volume (NVT) Monte Carlo simulation. After 2×10^5 sweeps, the adhesive square-well potential is switched on. For various values of ϕ and n_{lr}, simulations are performed with a set of different adhesion strengths ε. Additionally, for each choice of ϕ and n_{lr}, simulations were performed for systems with different numbers of rods N_r in order to examine finite-size effects. The number of sweeps required to equilibrate the system ranges from 4×10^6 to 2×10^7, depending on the rod volume fraction and the crosslinker concentration. After the system was equilibrated, averages were taken, using the same number of sweeps as for equilibration.

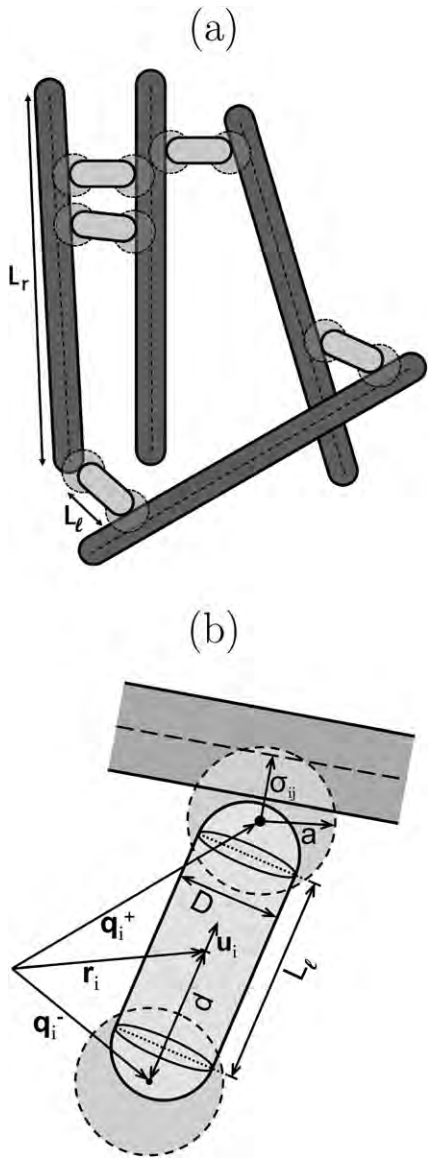

Fig. 1 (a) Binary system of spherocylinders inspired by the cytoskeleton: The rods are approximated by hard spherocylinders of length L_r and the crosslinkers by spherocylinders of length L_l with a rod-adhering site on each end. Rods and crosslinkers are taken to have the same diameter D. (b) Schematic representation of a crosslinker: The crosslinker has a center of mass $\mathbf{r}_i$ and a cylinder axis parallel to the unit vector $\mathbf{u}_i$. On the cylinder axis, two adhesive sites are located symmetrically at points $\mathbf{q}_i^+$ and $\mathbf{q}_i^-$ with a distance d to the center of mass. The adhesion sites interact with rods *via* square-well potentials of range a, while σ_{ij} is the distance between the rod axis and the nearest adhesion site.

2.1 Lifetime distribution of crosslinker contact

In simulations of cluster-forming systems, it is important to ensure that the configuration space is adequately sampled. For this purpose, we have investigated the lifetime distribution of rod–crosslinker contacts. The Monte Carlo sweeps between attachment and detachment of any crosslinker–rod pair are counted, and registered in a histogram. The normalized histogram gives the lifetime distribution $P(\tau)$. The lifetime distributions of the system are compared in Fig. 2 for $\varepsilon = 2.5T$ and $\varepsilon = 10T$ (here and below the Boltzmann constant is absorbed into the symbol T, *i.e.*, temperature is measured in energy units). For both adhesive strengths, the distribution is well described by an exponential form $\exp(-\alpha t)$ with $\alpha \simeq 0.21$ and $\alpha \simeq 0.13$ for $\varepsilon =$

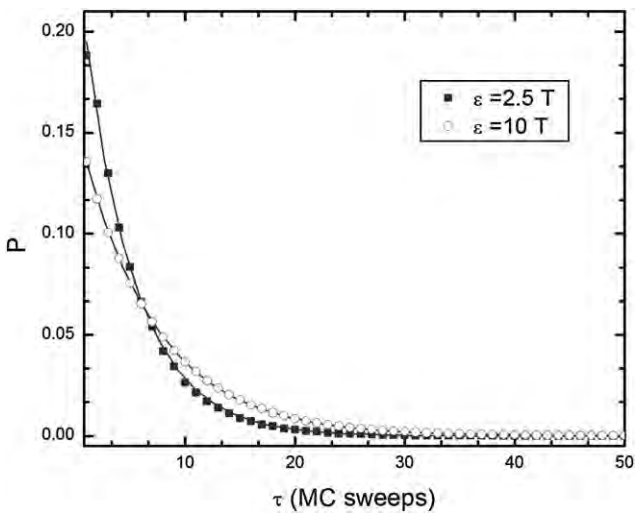

Fig. 2 Distribution P of lifetimes τ for the crosslinker–rod contacts in units of Monte Carlo sweeps at adhesive strengths $\varepsilon = 2.5T$ and $\varepsilon = 10T$.

$2.5T$ and $\varepsilon = 10T$, respectively. Summing the lifetime distribution up to $\tau = 20$ reveals that more than ninety percent of the contacts detach within 20 Monte Carlo sweeps. For both adhesion strengths shown in Fig. 2, $P(\tau)$ is essentially zero for $\tau \gtrsim 40$.

3. Percolating clusters

Using Monte Carlo simulations, the system is analyzed for various parameter values. In the absence of attractive interactions, *i.e.* for $\varepsilon = 0$, the rods and crosslinkers form an isotropic fluid. With increasing ε, the number of crosslinkers adhering to rods increases. Each crosslinker can bind up to two rods, one at each rod adhering site. In the following, two rods are called 'connected' if they bind to the same crosslinker. A pair of rods can be connected by one or several crosslinkers. A rod can be connected to several other rods. For a given configuration the rods are divided into groups called *clusters*. A rod is part of a cluster, if it is connected to, at least, one rod belonging to the cluster. The size of a cluster is taken to be the number of rods in the cluster. Choosing values of $\phi \gtrsim 0.02$ and $n_{lr} \gtrsim 1$, we find a threshold value of ε above which the clusters percolate and form a space-filling network. Previous studies have shown that the percolated phase of an actin-linker system is of the generic sol-gel type.[22,27] Sol-gel transitions have been successfully studied with percolation theory.[42–44] In the following, we use methods of percolation theory to investigate the structure of our model system.

In percolation theory, one considers an infinite system in which clusters of different sizes may form. A percolation transition is marked by the formation of an infinitely large cluster, which spans the entire system. In a finite system, the divergence of the size of one cluster is replaced by a strong growth of one cluster while the other clusters shrink. The fraction of monomers belonging to the largest cluster can be used as an order parameter. Let n_s be the probability that an arbitrary cluster in an infinitely large system has the size s. Based on scaling arguments, the cluster size distribution n_s has the general form,[43,44]

$$n_s \propto s^{-\tau} f[(p - p_c)s^{\sigma}]. \tag{6}$$

where p is the probability that a pair of rods is connected. Note that the cluster size distribution differs from the bundle size distribution which is based on the number of almost parallely oriented rods that form a bundle. The bundling behavior of the system is investigated in Sec. 4.

At the critical attachment probability p_c, n_s is predicted to have a power law decay,[43,44]

$$n_s(p_c) \propto s^{-\tau} \tag{7}$$

where τ is called the Fisher exponent.[43,44] A useful quantity is the second moment of n_s, which is defined as

$$M_2 \equiv \sum_{s=1}^{s_m - 1} s^2 n_s \tag{8}$$

where the sum goes over all cluster sizes which are smaller than the size of the largest cluster s_m. For $p \approx p_c$, M_2 scales like[43,44]

$$M_2 \propto |p - p_c|^{(\tau - 3)/\sigma}. \tag{9}$$

The exponent of M_2 is determined by two parameters, the Fisher exponent τ and another critical exponent σ.

3.1 Simulation results

At very low ε, the rods and crosslinkers are in an isotropic fluid state. As ε is increased, a growing fraction of crosslinkers is attached to rods. Increasing ε also leads to an increasing number of connected rods, which causes the formation of clusters. For moderate ε, the clusters are of comparable size. The average cluster size increases with ε. Let us assume that the percolation threshold of an infinite system occurs at $\tilde{\varepsilon}(\phi, n_{lr})$. In the simulations, the second moment of the cluster size distribution M_2 has been measured by counting the number of rods in each cluster. It shows a continuous increase with ε until $\varepsilon \simeq \tilde{\varepsilon}(\phi, n_{lr})$, where one large cluster emerges in the system, whose size is distinctly larger than that of all the other clusters. If ε is increased further, a growing number of rods are incorporated into the spanning cluster. As a consequence, the value of M_2, which includes all clusters apart from the largest one, decreases again.

With increasing system size, the location $\varepsilon = \varepsilon_{max}$ of the maximum of $M_2(\varepsilon)$ converges to the percolation threshold $\tilde{\varepsilon}(\phi, n_{lr})$ of an infinite system.[45–47] In Fig. 3, we show plots of M_2 as a function of ε for $\phi = 0.03$, $n_{lr} = 2$, and different system sizes. For the tested system sizes, the obtained value of ε at which M_2 attains its maximum does not change significantly.

Another measurable quantity which indicates a percolation transition is the average fraction of rods that belong to the largest cluster, $\langle s_{max} \rangle$, which is also treated as an extensive order parameter.[47,48] For a sufficiently large cluster the percolation transition occurs at the value of ε at which $\langle s_{max} \rangle = 0.5$. As shown in Fig. 4(b) and Fig. 5(b), $\langle s_{max} \rangle$ increases continuously from 0 to 1, as a spanning cluster forms in the system. The maximum of M_2 coincides well with the value of ε at which the largest cluster consists of approximately 50% of the rods. The system has been analyzed for a fixed rod volume fraction ϕ and different values of the crosslinker–rod ratio n_{lr}, by varying the adhesive strength ε. Fig. 4(a) and Fig. 4(b) show results of M_2 and $\langle s_{max} \rangle$, respectively, as a function of ε for $\phi = 0.03$. As n_{lr} is increased from 1.3 to 6, the maximum M_2 is shifted gradually to lower values of ε. As shown in Fig. 4(b), the criterion $\langle s_{max} \rangle = 0.5$ provides transition values for ε that are quite similar to the ones obtained from the maxima of M_2.

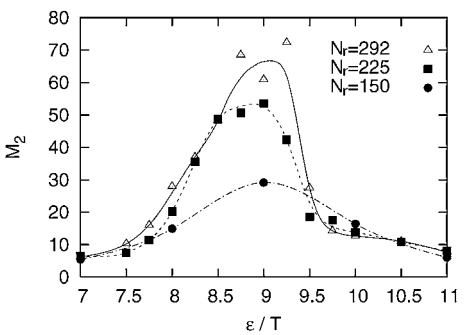

Fig. 3 The second moment of the cluster size distribution, M_2, as a function of the adhesive strength ε for various rod numbers N_r at a fixed rod volume fraction $\phi = 0.03$ and a crosslinker–rod ratio $n_{lr} = 2$. Lines are intended to guide the eye.

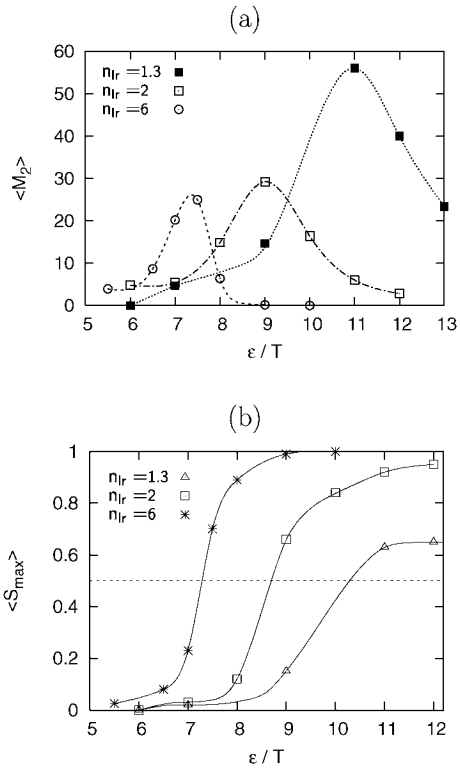

Fig. 4 (a) The second moment of the cluster size distribution, M_2, for a rod volume fraction $\phi = 0.03$, as a function of the adhesive strength ε. Different symbols represent different values of the crosslinker–rod ratio n_{lr}. (b) The average fraction of rods $\langle s_{max} \rangle$ that are part of the largest cluster as a function of the adhesive strength ε for a rod volume fraction $\phi = 0.03$. The horizontal dotted line denotes $\langle s_{max} \rangle = 0.5$. Different symbols represent different values of the crosslinker–rod ratio n_{lr}. Lines are intended to guide the eye.

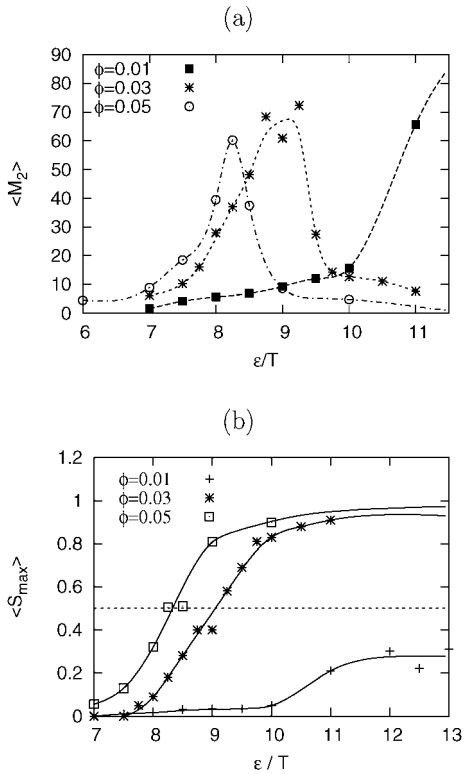

Fig. 5 (a) The second moment of the cluster size distribution, M_2, as a function of the adhesive strength ε for a crosslinker–rod ratio $n_{lr} = 2$ and different values of the rod volume fraction ϕ. (b) The fraction of rods included in the largest cluster $\langle s_{max} \rangle$ for crosslinker–rod ratio $n_{lr} = 2$ and various values of the rod volume fraction ϕ. The horizontal dotted line denotes $\langle s_{max} \rangle = 0.5$. Lines are intended to guide the eye.

Fig. 5(a) and Fig. 5(b) show average values of M_2 and s_{max} for systems with crosslinker–rod ratio $n_{lr} = 2$ and different rod volume fraction ϕ as a function of the adhesive strength ε. For $\phi \lesssim 0.01$, the value of M_2 increases with ε, but a maximum has not been reached within the observed range of ε. For large ε, $\langle s_{max} \rangle$ appears to saturate to a value distinctly lower than one. For larger ϕ, Fig. 5(a) shows a peak for M_2. With increasing rod volume fraction ϕ, the peak of M_2 is shifted towards lower values of ε, indicating that a spanning cluster forms already at lower values of ε. In Table 1, the threshold values of ε obtained with the two criteria are compared for $n_{lr} = 2$ and $n_{lr} = 6$ at different values of the rod volume fraction ϕ. For infinitely large systems, both ε values are predicted to coincide with the percolation threshold $\tilde{\varepsilon}$. The data obtained for the different system sizes indicate that the obtained threshold values depend only weakly on system size.

According to Eq. 8, the cluster size distribution n_s should fit to a power-law decay, close to the transition point. In Fig. 6(a), double logarithmic plots of $p(s)$ for a system with $\phi = 0.03$, $n_{lr} = 2$, and $\varepsilon = 9T$ are shown together with the best power-law fit. Since the largest cluster size is limited by the system size, $p(s)$ deviates from power-law behavior at large s, where it shows a peak, close to N_s, the total number of rods in the system. The peak region of the cluster size distribution is excluded from the power-law fit, which then gives a Fisher exponent, $\tau \simeq 2.5$ for $\phi = 0.03$ and $n_{lr} = 2$.

Table 1 Values of the reduced adhesion strength ε/T obtained at the maximum of $M_2(\varepsilon)$ and at $\langle s_{max} \rangle(\varepsilon) \simeq 0.5$ for different values of the rod volume fraction ϕ and crosslinker–rod ratio n_{lr}. For large systems, both ε values approach the percolation threshold $\tilde{\varepsilon}$

n_{lr}	ϕ	ε/T at maximum of M_2	ε/T at $\langle s_{max} \rangle \simeq 0.5$
2	0.02	11	10.5
2	0.03	9	9.25
2	0.05	8.25	8.5
6	0.02	8.5	8.5
6	0.03	7.5	7.5
6	0.04	7.0	7.25
6	0.05	6.75	6.75

Recently, the percolation of carbon nanotubes in polymeric and colloidal media has been studied analytically.[38] The study shows that the percolation threshold depends sensitively on the length distribution and the attractive interactions between the nanotubes. Similar results have been found in Monte Carlo simulations of spherocylinders with an effective adhesion induced by depletion forces.[39] No such information exists about the Fisher exponent which, to the best of our knowledge, has not been calculated so far.

For the similar problem of randomly branching polymers two universality classes have been found, for which the Fisher exponent is universal (see ref. 49). For polymerization processes of small multifunctional monomers, the Fisher exponent can be

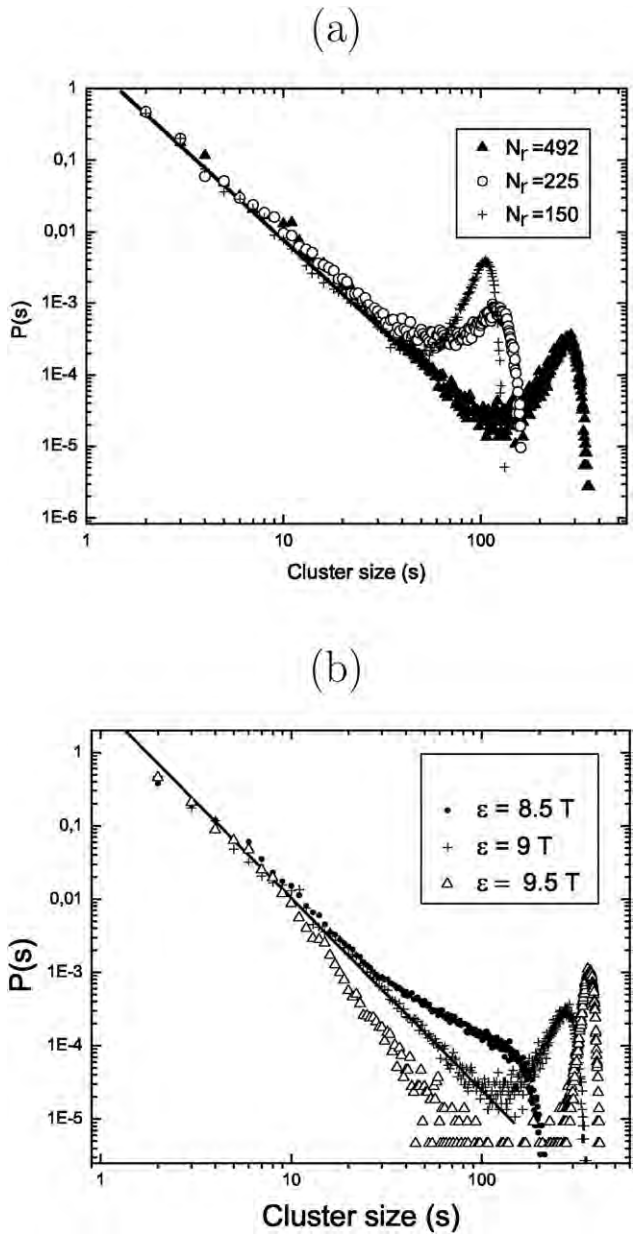

Fig. 6 (a) Distribution $P(s)$ of the cluster size s for a rod volume fraction $\phi = 0.03$ and an adhesive strength $\varepsilon = 9T$. Different symbols represent different system sizes. The line represents a fit corresponding to a power law decay as in Eq. 8 with exponent $\tau = 2.5 \pm 0.03$. (b) Cluster size distribution $P(s)$ for a rod volume fraction $\phi = 0.03$, a crosslinker–rod ratio $n_{lr} = 2$ and a number of rods $N_r = 492$. Different symbols stand for different values ε. The line is identical to that in Fig. 6(a).

obtained from percolation theory and has a value of $\tau \simeq 2.2$. Systems with long chain segments between the branching points belong to the *vulcanization* class[50] and behave like a system of long linear polymers that are crosslinked by short agents. For this class, the width of the critical percolation region is almost zero and, close to the percolation threshold, the cluster size distribution is described by the Flory-Stockmayer theory,[51–53] which predicts a Fisher exponent of $\tau = 2.5$.[54] Both exponents are universal in the limit of long and short polymer segments between branch points. For a polymer system that lies in the crossover regime of the two classes, an intermediate value of $\tau \simeq 2.35$ has been measured.[42,54] With a Fisher exponent of $\tau = 2.5$ our system appears to belong to the vulcanization class, but one has to keep in mind that the approach by de Gennes considers randomly curved polymers and does not consider parallel alignment of multiply connected polymers or rods.

The cluster size distribution n_s is compared for systems with three different ε in Fig. 6(b). The best power-law behavior is found for $\varepsilon = 9T$. For $\varepsilon = 8.5T$ and $9.5T$, the distribution n_s shows a larger deviation at higher cluster sizes. This indicates that the threshold value is approximately $\tilde{\varepsilon}(\phi = 0.03, n_{lr} = 2) \simeq 9T$, which is in good agreement with the value found with the other two criteria, as listed in Table 1.

4. Bundles

If two rods are interconnected by more than two crosslinkers, the rod axes have to be fairly parallel. Therefore, bundles of approximately parallel rods may occur in the system. This phenomenon is similar to the bundling of intra-cellular filaments in the presence of interconnecting proteins.[16] Tempel *et al.*[22] have proposed a phase diagram of a system of actin filaments and α-actinin linkers, in which the bundling phenomenon appears for high linker density regions. In the region of lower α-actinin densities, they propose a transition of the sol-gel type, where the transition line denotes the threshold of the crosslinker concentration below which the presence of the crosslinkers has no influence on the structure of the filament system. Pelletier *et al.*[55] reported on the formation of 3D networks of bundles in a system of F-actin and α-actinin, based on small-angle X-ray scattering and laser scanning confocal microscopy. A crosslinker induced bundling of filaments is also predicted by an analytical model, based on the Onsager theory.[26] The unbinding of filament bundles was also studied by Kierfeld *et al.*[56] For a system of actin filaments and crosslinkers, the formation of bundles may be affected by several phenomena that are not included in our model system. The size of filament bundles may be influenced by the growth dynamics of actin filaments,[57] by the presence of counterion-induced long-range interactions[40,41] or by a chiral conformation of filaments in a bundle.[58] Our model system considers uncharged rigid filaments of fixed length, so that the degree of bundling reflects the interplay between the crosslinker-mediated filament–filament interactions and entropic effects.

With the help of Monte Carlo simulations, we have studied the occurrence of rod bundling in our model system. The formation of bundles depends on all three system parameters, ϕ, n_{lr}, and ε. Bundling is found in dilute systems as well as in percolating networks. The typical structure of bundles in a system with a low rod volume fraction is presented in Fig. 7(a). It shows small clusters of aligned rods, which are strongly interconnected by crosslinkers. A typical configuration of a spanning network with pronounced bundling is shown in Fig. 7(b).

In our simulations, bundling is detected by measuring the mutual alignment of connected rods. We define two connected rods i and j to be in the same bundle if they are aligned almost parallel to each other. More precisely, the angle between the rod axes θ_{ij} must satisfy the condition $|\cos \theta_{ij}| \geq 0.95$. The fraction $\langle n_b \rangle$ of rods involved in any bundle is used to indicate the extent of bundling within the system.

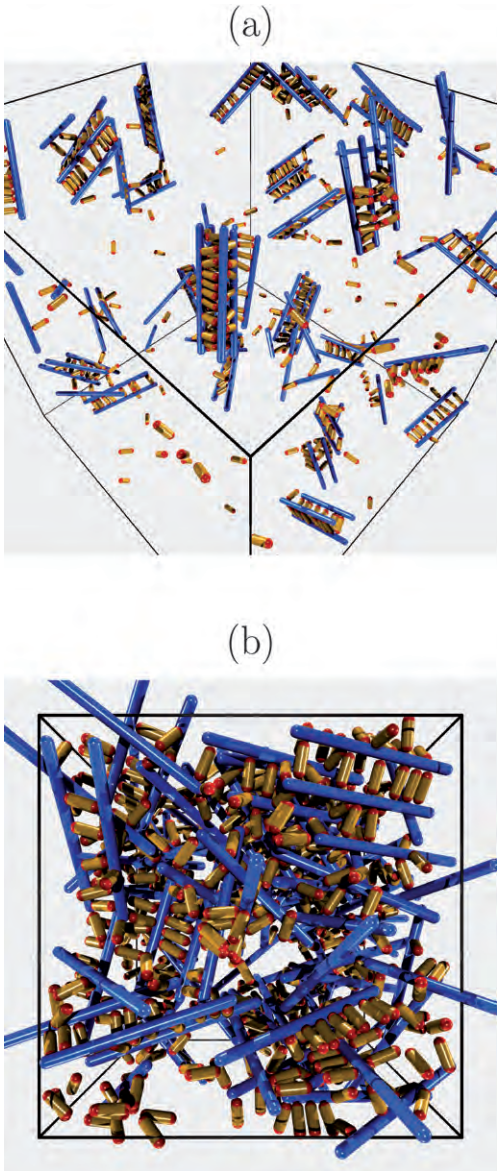

Fig. 7 (a) A typical configuration for a system with volume fraction $\phi = 0.003$, crosslinker–rod ratio $n_{lr} = 6$, and adhesive strength $\varepsilon = 10T$. The rods do not form a spanning cluster. The majority of rods form crosslinker-induced bundles. (b) A typical configuration of a percolating network that includes bundles of parallel rods. The figure shows a system with a rod volume fraction $\phi = 0.03$, a crosslinker–rod ratio $n_{lr} = 9$, and an adhesive strength $\varepsilon = 10T$.

Bundling has also been studied with the help of the orientational pair correlation function

$$g_2(r) \equiv \left\langle \frac{\sum_{i \neq j} P_2(\cos\theta_{ij})\,\delta(r - r_{ij})}{\sum_{i \neq j} \delta(r - r_{ij})} \right\rangle \tag{10}$$

where

$$P_2(\cos\theta_{ij}) = \frac{3}{2}\cos^2\theta_{ij} - \frac{1}{2} \tag{11}$$

is the second Legendre polynomial and the delta function restricts the sampling to pairs of rods i and j with a distance $r_{ij} = r$ between the centers of mass. Numerically, the delta function is realized by selecting small, finite intervals $[r - \Delta/2, r + \Delta/2)$ of width Δ. For structures with pronounced bundling, $g_2(r)$ shows distinct oscillations, which decrease with increasing r. These oscillations result from the ordered packing of almost parallel rods. In Fig. 8, examples of $g_2(r)$ are presented. For $n_{lr} = 6$ and $\phi = 0.003$, oscillations in $g_2(r)$ are more pronounced than for $n_{lr} = 2$ and $\phi = 0.01$, where bundling effects are weaker. For a system with $n_{lr} = 2$ and $\phi = 0.05$, the fraction $\langle n_b \rangle$ of rods that form bundles is low and $g_2(r)$ has only one distinct maximum.

We have systematically studied the fraction $\langle n_b \rangle$ of rods involved in bundles as a function of the system parameters. As one would assume, $\langle n_b \rangle$ increases with increasing crosslinker–rod ratio. The dependence of $\langle n_b \rangle$ on ϕ and ε is, however, less intuitive. This is demonstrated in Fig. 9, where $\langle n_b \rangle$ is shown as a function of ε for $n_{lr} = 2$ and various rod volume fraction values ϕ. For high ε, the bundling effect is generally weakened if the rod volume fraction ϕ is increased. This effect can be explained by recalling that it is energetically favorable if both ends of the

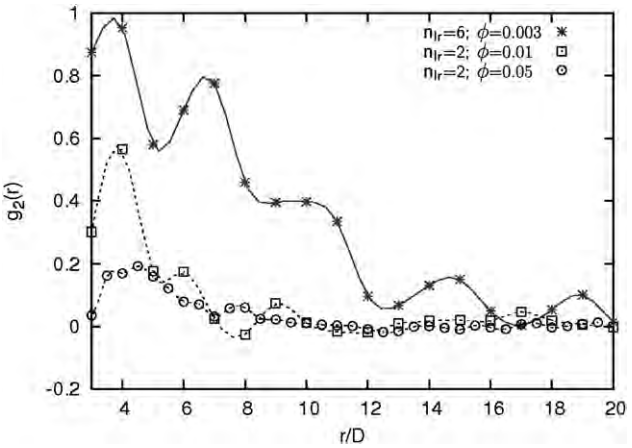

Fig. 8 The orientational correlation function $g_2(r)$ as a function of the rod distance r for an adhesive strength $\varepsilon = 10T$. Results are shown for different values of the rod volume fraction ϕ and the crosslinker–rod ratio n_{lr}. Strong oscillations of $g_2(r)$ are correlated with pronounced bundling. Lines are intended to guide the eye.

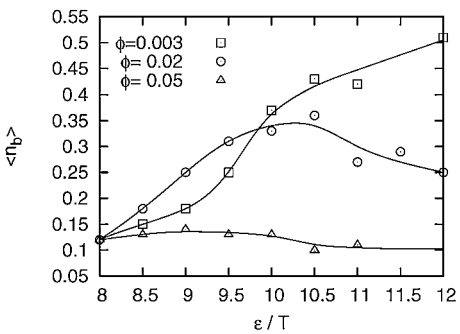

Fig. 9 The fraction of rods forming bundles $\langle n_b \rangle$ for a fixed crosslinker–rod ratio $n_{lr} = 2$, measured as a function of the adhesive strength ε. Different symbols represent different values of rod volume fractions ϕ. Bundling diminishes with increasing rod volume fraction ϕ. For $\phi = 0.02$, $\langle n_b \rangle$ is a non-monotonic function of ε. Lines are intended to guide the eye.

crosslinkers bind to rods. At low rod concentrations, small isolated rod bundles are required to create adhesion on both ends of the crosslinkers. With increasing ϕ the network of rods gets more dense so that a sufficient number of crosslinks may form between non-aligned rods. For $\phi = 0.003$ the fraction of bundling rods increases monotonically with ε while for $\phi = 0.05$, bundling is basically absent. A particularly interesting system behavior is found for $\phi = 0.02$. Here, rods form a spanning network at $\varepsilon \sim 10.5T$. For $\varepsilon \lesssim 8.5T$, the system is in an isotropic fluid state, and the fraction of bundling rods is very low. With increasing ε, $\langle n_b \rangle$ increases and reaches a maximum $\langle n_b \rangle \simeq 0.33$ at $\varepsilon \simeq 10.5T$, above which it decreases distinctly. The maximum of $\langle n_b \rangle$ corresponds well with the percolation threshold for the given values of ϕ and n_{lr}. Apparently, the bundling is diminished by the formation of a spanning network, in which many non-aligned rods can be crosslinked.

5. Phase diagrams

In this section, an overview of the structural properties of the system is given in terms of "phase diagrams". The system has been analyzed for values of ϕ ranging from 0.003 to 0.05, for n_{lr} in the range of 0.5 to 6, and for ε values ranging from $6T$ to $15T$.

In order to analyze the influence of the system parameters on the bundling behavior, we define a criterion for "substantial bundling" in a system. Generally, one finds that the orientational correlation function $g_2(r)$ shows distinct oscillations for systems with $\langle n_b \rangle \geq 0.2$, in which more than 20% of rods form bundles. For $\langle n_b \rangle \ll 0.2$, the orientational correlation function has basically one peak. In the following, a system with $\langle n_b \rangle > 0.2$ is said to belong to a *bundling region* in the parameter space spanned by ϕ, n_{lr}, and ε.

The properties of the system depend on the three independent control parameters, ϕ, n_{lr}, and ε, and it is useful to draw more than one phase diagram, in order to summarize the results obtained for different parameter values. The phase diagram in Fig. 10 has been constructed by fixing the rod volume fraction $\phi = 0.03$ and shows the dependence of the rod assembling structure on the crosslinker–rod ratio n_{lr} and the adhesive strength of the crosslinkers ε. Fig. 11 shows a phase diagram of ϕ and ε, for a fixed crosslinker–rod ratio $n_{lr} = 2$.

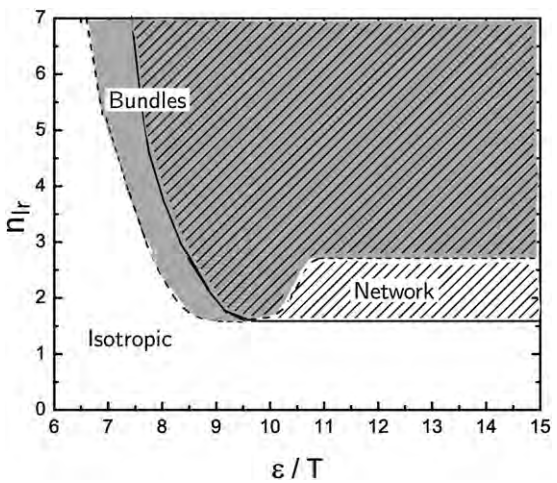

Fig. 10 Phase diagram as a function of adhesive strength ε and crosslinkers per rod n_{lr} for rod volume fraction $\phi = 0.03$. The diagram contains two different boundary lines. First, the percolation threshold (solid line) separates the isotropic phase from the percolating network phase (shaded). Second, the threshold of substantial bundling (dashed line) separates configurations with many bundles (grey) from those for which bundles are rare. Outside the grey shaded region, less then 20% of the rods are involved in a bundle.

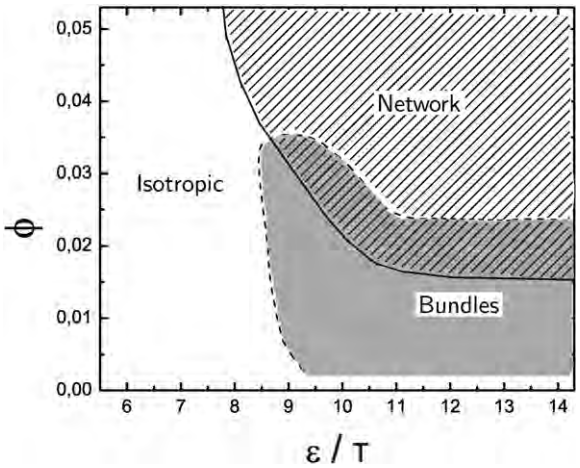

Fig. 11 Phase diagram as a function of adhesive strength ε and volume fraction ϕ for crosslinker–rod ratio $n_{lr} = 2$. The rods form bundles (grey region) and spanning clusters (shaded region) for certain parameter regions. As in Fig. 10, the percolation threshold is indicated by the solid line and the threshold of substantial bundling by the dashed one.

5.1 Constant rod volume fraction ϕ

For volume fractions $\phi = 0.03$, the system has been analyzed for values of n_{lr} ranging from 0.5 to 6.0 and ε ranging from 0 to $15T$. The results are summarized in Fig. 10, where the shaded (hatched) area denotes the region of percolated states and the percolation transition line is indicated by the solid line. Substantial bundling is found within the grey region, which is bounded by the dashed line. For $n_{lr} < 1.5$, the rods do not form networks or bundles within the analyzed range of ε. A percolated network is found for $n_{lr} \gtrsim 1.5$, if ε is sufficiently large. As n_{lr} is increased, the percolation boundary is shifted to lower values of ε. As indicated by the dashed line in Fig. 10, substantial bundling sets in for ε values below the percolation threshold. For large crosslinker–rod ratios $n_{lr} \gtrsim 2$, percolated networks include a substantial amount of bundles over the whole range of ε, observed. In contrast, for $n_{lr} = 2$, bundling is maximal at $\varepsilon \simeq 8.0T$ and less than 20% of the rods form bundles for $\varepsilon \gtrsim 10.5T$. An explanation for this non-monotonic behavior of the fraction $\langle n_b \rangle = \langle n_b \rangle(\varepsilon)$ has been given in the last section.

5.2 Fixed crosslinker concentration

For a fixed value of the crosslinker–rod ratio $n_{lr} = 2$, the system has been analyzed for rod volume fractions ϕ ranging from 0.003 to 0.05 and various adhesive strengths ε. The properties are summarized in Fig. 11. Within the observed range of ε, spanning networks are not observed for $\phi \lesssim 0.01$. However, bundles are formed by rods at these values of ϕ, when ε is sufficiently high. Space-filling networks are observed in systems with $\phi \gtrsim 0.02$ at

sufficiently large values of ε. As ϕ is increased, the percolation boundary is shifted to lower values of ε. In the range $0.025 \lesssim \phi \lesssim 0.03$, the amount of rods included in bundles is a non-monotonic function of ε with a maximum close to the percolation boundary. Substantial bundling is suppressed for $\phi \gtrsim 0.035$. Within an intermediate region, with $0.02 \lesssim \phi \lesssim 0.03$, substantial bundling is found in a space-filling network.

6. Summary

With the help of Monte Carlo simulations, we have analyzed a simple model system of rods and crosslinkers. Our simulation study reveals a complex dependence of the properties of the system on rod volume fraction, crosslinker concentration and the affinity of the crosslinkers.

The rods form a space-filling network if the rod volume fraction ϕ, the crosslinker–rod ratio n_{lr}, and the adhesion strength ε are sufficiently large.

The fraction $\langle n_b \rangle$ of rods that are part of an aligned bundle increases with increasing crosslinker–rod ratio n_{lr}, but decreases with increasing rod volume fraction ϕ. This behaviour agrees qualitatively with the phase diagram in ref. 26, which was obtained for the case of an effective crosslinking potential that does not depend on the rod alignment. In a certain parameter range of n_{lr} and ϕ, the fraction $\langle n_b \rangle$ of bundling rods is a non-monotonic function of the adhesion strength ε and has a maximum close to the percolation boundary.

Percolation and substantial bundling can be found in all combinations. For low crosslinker–rod ratios and adhesion strengths the system is in an isotropic, fluid state. For sufficiently low rod volume fractions, isolated bundles of aligned rods are found. Furthermore, the investigated system forms percolated states with and without substantial bundling.

The bundling behavior can be understood in the following way. For sufficiently large adhesion strength, crosslinkers tend to bind rods on both ends. In a dense percolated system, resulting from large ϕ and ε, each rod has a comparatively large number of different neighboring rods. As a consequence, crosslinkers that bind to the same rod typically do not share the same rod on the other end. Since sharing several crosslinkers is the underlying mechanism for the formation of bundles, bundling in dense percolated systems is reduced.

The simulations described here have been restricted to one crosslinker length. As shown in ref. 17, the length of the crosslinkers has a strong influence on the structural and mechanical properties of an actin network. It would be interesting to investigate these effects in future simulation studies.

Finally, we would like to mention that the gel-like network state is different from an isotropic fluid state in terms of mechanical properties. An interesting task for future investigations would be to study system properties such as the elastic modulus and to determine whether there are thermodynamic phase transitions between the different structures formed by the system.

References

1 P. G. Bolhuis and D. Frenkel, *J. Chem. Phys.*, 1997, **106**, 666.
2 H. N. W. Lekkerkerker, P. Coulon, R. van der Haegen and R. Deblieck, *J. Chem. Phys.*, 1984, **80**, 3427.
3 R. P. Sear and B. M. Mulder, *J. Chem. Phys.*, 1997, **106**, 3827.
4 M. Dijkstra and R. van Roij, *Phys. Rev. E*, 1997, **56**, 5594.
5 R. van Roij, B. Mulder and M. Dijkstra, *Physica A*, 1998, **261**, 374.
6 H. Bosetti and A. Perera, *Phys. Rev. E*, 2001, **63**, 021206.
7 P. C. Hemmer, *J. Stat. Phys.*, 2000, **100**, 3.
8 G. Cinacchi, L. Mederos and E. Velasco, *J. Chem. Phys.*, 2004, **121**, 3854.
9 G. Cinacchi, Y. Martínez-Ratón, L. Mederos and E. Velasco, *Mol. Cryst. Liq. Cryst.*, 2007, **465**, 121.
10 J. Janeček and T. Boublík, *Mol. Phys.*, 2006, **104**, 197.
11 S. C. McGrother, R. P. Sear and G. Jackson, *J. Chem. Phys.*, 1997, **106**, 7315.
12 R. Chelakkot, R. Lipowsky and T. Gruhn, *Macromolecules*, 2006, **39**, 7138.
13 M. Hazani, D. Shvarts, D. Peled, V. Sidorov and R. Naaman, *Faraday Discuss.*, 2006, **131**, 325.
14 G. Gruner, *Anal. Bioanal. Chem.*, 2006, **384**, 322.
15 A. Star, V. Joshi, S. Skarupo, D. Thomas and J.-C. P. Gabriel, *J. Phys. Chem. B*, 2006, **110**, 21014.
16 H. Lodish, P. Matsudaira, A. Berk, S. L. Zipursky, J. Darnell, H. F. Lodish, C. A. Kaiser, M. Krieger, M. P. Scott and M. Sahimi, *Molecular Cell Biology*, W.H. Freeman & Co, San Francisco, fifth ed., 2003.
17 B. Wagner, R. Tharmann, I. Haase, M. Fischer and A. R. Bausch, *Proc. Nat. Acad. Sci. USA*, 2006, **103**, 13974.
18 P. A. Janmey, S. Hvidt, J. Lamb and T. P. Stossel, *Nature*, 1990, **345**, 89.
19 M. L. Gardel, J. H. Shin, F. C. MacKintosh, L. Mahadevan, P. Matsudeira and D. A. Weitz, *Science*, 2004, **304**, 1301.
20 J. H. Shin, M. L. Gardel, L. Mahadevan, P. Matsudaira and D. A. Weitz, *Proc. Nat. Acad. Sci. USA*, 2004, **101**, 9636.
21 D. H. Wachsstock, W. H. Schwarz and T. D. Pollard, *Biophys. J.*, 1993, **64**(2), A148.
22 M. Tempel, G. Isenberg and E. Sackmann, *Phys. Rev. E*, 1996, **54**(2), 1802.
23 S. Inoue and E. D. Salmon, *Mol. Biol. Cell*, 1995, **6**(12).
24 C. G. D. Remedios, D. Chhabra, M. Kekic, I. V. Dedova, M. Tsubakihara, D. A. Berry and N. J. Nosworthy, *Physiol. Rev.*, 2003, **83**(2), 433.
25 J. Kierfeld and R. Lipowsky, *Europhys. Lett.*, 2003, **62**(285).
26 L. Borukhov, R. F. Bruinsma, W. M. Gelbart and A. J. Liu, *Proc. Nat. Acad. Sci. USA*, 2005, **102**(10), 3673.
27 A. G. Zilman and S. A. Safran, *Europhys. Lett.*, 2003, **63**(1), 139.
28 P. Kraikivski, R. Lipowsky and J. Kierfeld, *Phys. Rev. Lett.*, 2006, **96**(258103).
29 F. Ziebert and W. Zimmermann, *Phys. Rev. E*, 2004, **70**(2).
30 H. Y. Lee and M. Kardar, *Phys. Rev. E*, 2001, **64**(5), 056113.
31 T. Surrey, F. Nedelec, S. Leibler and E. Karsenti, *Science*, 2001, **292**(5519), 1167.
32 F. J. Nedelec, T. Surrey, A. C. Maggs and S. Leibler, *Nature*, 1997, **389**(6648), 305.
33 D. Sept, A. H. Elcock and J. A. McCammon, *J. Mol. Biol.*, 1999, **294**(5), 1181.
34 D. Sept and J. A. McCammon, *Biophys. J.*, 2001, **81**(2), 667.
35 A. Ott, M. Magnasco, A. Simon and A. Libchaber, *Phys. Rev. E*, 1993, **48**, R1642.
36 D. Biron and E. Moses, *Biophys. J.*, 2004, **86**, 3284.
37 N. Gov, *Europhys. Lett.*, 2007, **77**, 68005.
38 A. Kyrylyuk and P. van der Schoot, *Proc. Natl. Acad. Sci. USA*, 2008, **105**, 8221.
39 T. Schilling, S. Jungblut and M. Miller, *Phys. Rev. Lett.*, 2007, **98**, 108303.
40 M. Henle and P. A. Pinkus, *Phys. Rev. E*, 2005, **71**, 060801.
41 K. Shikinaka, H. Kwon, A. Kakugo, H. Furukawa, Y. Osada and J. P. Gong, *Biomacromolecules*, 2008, **9**, 537.
42 R. H. Colby, J. R. Gillmor and M. Rubinstein, *Phys. Rev. E*, 1993, **48**(5), 3712.
43 D. Stauffer and A. Aharony, *Introduction to percolation theory*, Taylor and Francis, London, first ed., 1992.
44 M. Sahimi, *Applications of percolation theory*, Taylor and Francis, London, first ed., 1994.
45 X. Campi, *J. Phys. A: Math. Gen.*, 1986, **19**(15), L917.
46 J. B. Elliott, *Phys. Rev. C*, 2000, **6206**(6).
47 Y. Liu and R. B. Pandey, *J. Chem. Phys.*, 1996, **105**(2), 825.
48 J. Brzychczyk, *Phys. Rev. C*, 2006, **73**(2).

49 C. Lusignan, T. Mourey, J. Wilson and R. Colby, *Phys. Rev. E*, 1999, **60**, 5657.
50 P. de Gennes, *J. Phys: (Paris) Lett.*, 1977, **38**, L355.
51 P. Flory, *J. Amer. Chem. Soc.*, 1941, **63**, 3083.
52 P. Flory, *J. Amer. Chem. Soc.*, 1941, **63**, 3091.
53 W. Stockmayer, *J. Chem. Phys.*, 1943, **11**, 45.
54 R. H. Colby, J. R. Gillmor and M. Rubinstein, *Macromolecules*, 1992, **25**, 7180.
55 O. Pelletier, E. Pokidysheva, L. S. Hirst, N. Bouxsein, Y. Li and C. R. Safinya, *Phys. Rev. Lett.*, 2003, **91**(14).
56 J. Kierfeld, T. Kuhne and R. Lipowsky, *Phys. Rev. Lett.*, 2005, **95**(3).
57 L. Haviv, N. Gov, Y. Ideses and A. Bernheim-Groswasser, *Eur. Biophys. J.*, 2008, **37**, 447.
58 G. M. Grason and R. F. Bruinsma, *Phys. Rev. Lett.*, 2007, **99**, 098101.